

Impact of Cloud Cover on Solar Radiative Biases in Deep Convective Regimes

F. DI GIUSEPPE

ARPA Servizio IdroMeteorologico, Bologna, Italy

A. M. TOMPKINS

ECMWF, Reading, United Kingdom

(Manuscript received 2 July 2004, in final form 29 September 2004)

ABSTRACT

Conflicting claims have been made concerning the magnitude of the bias in solar radiative transfer calculations when horizontal photon transport is neglected for deep convective scenarios. The difficulty of obtaining a realistic set of cloud scenes for situations of complex cloud geometry, while certain characteristics such as total cloud cover are systematically controlled, has hindered the attempt to reach a consensus. Here, a simple alternative approach is adopted. An ensemble of cloud scenes generated by a cloud resolving model are modified by an idealized function that progressively alters the cirrus anvil coverage without affecting the realism of the scene produced. Comparing three-dimensional radiative calculations with the independent column approximation for all cloud scenes, it is found that the bias in scene albedo can reach as much as 22% when the sun is overhead and 46% at low sun angles. The bias is an asymmetrical function of cloud cover with a maximum attained at cirrus anvil cloud cover of approximately 30%–40%. With a cloud cover of 15%, the bias is half its maximum value, while it is limited for coverage exceeding 80%. The position of the peak occurs at the cloud cover coinciding with the maximum number of independent clouds present in the scene. Increasing the cloud cover past this point produces a decrease in the number of isolated clouds because of cloud merging, with a consequential bias reduction.

With this systematic documentation of the biases as a function of total cloud cover, it is possible to identify two contributions to the total error: the geometrical consequences of the effective cloud cover increase at low sun angles and the true 3D scattering effect of photons deviating from the original path direction. An attempt to account for the former geometrical contribution to the 1D bias is made by performing a simple correction technique, whereby the field is sheared by the tangent of the solar zenith angle. It is found that this greatly reduces the 1D biases at low sun angles. Because of the small aspect ratio of the cirrus cloud deck, the remaining bias contribution is small in magnitude and almost independent of solar zenith angle.

1. Introduction

The neglect of horizontal photon transport in cloudy atmospheres could lead to significant biases in solar radiative heating rates. The magnitude of the bias will depend both on the spatial scale over which it is assessed and on the specific nature of the cloud regime. Previous studies have usually attempted to determine this bias by comparing separate radiative transfer calculations through a given cloud field, for which horizontal photon transport is successively inhibited and permitted. The large phase space of complex cloud regimes requiring investigation has led to conflicting assessments of this bias and its significance for parameterization in atmospheric models.

There is general agreement that for overcast single-layer cloud systems such as stratocumulus, 3D effects are minimal (Cahalan et al. 1994; Marshak et al. 1997; Di Giuseppe and Tompkins 2003a). Once such shallow clouds become broken this does not appear to be the case (McKee and Cox 1974; Aida 1977; Barker and Davies 1992; O'Hirok and Gautier 1998). In particular, Di Giuseppe and Tompkins (2003a) indicated that 3D effects in broken stratocumulus of 80% cover became relevant when the dominant horizontal spatial scale of the cloud fell below 5 km. This implies that GCMs that suffer from plane-parallel biases because of the neglected horizontal subgrid-scale variability of cloud water for such scenes could be making additional errors because of these 3D effects. Barker and Li (1997) also emphasized the role of 3D effects over shorter horizontal scales when discussing the purported cloud anomalous absorption effect. Significant biases are found analyzing cloud fields reconstructed from remote sensing

Corresponding author address: Francesca Di Giuseppe, ARPA-SIM, Viale Silvani, 6 I-40128 Bologna, Italy.
E-mail: fdigiuseppe@smr.arpa.emr.it

techniques (Chambers et al. 1997; Zuidema and Evans 1998)

For other cloud systems with more complex geometry, such as convective regimes, there is conflicting opinion. Vogelmann et al. (2001), using satellite data to reconstruct deep convective cloud fields, concluded that 3D effects could be significant, especially locally, broadly agreeing with O'Hirok and Gautier (1998). Other studies have instead used output from cloud resolving models (CRMs) to provide a proxy cloud field as the input for the radiative calculations. Di Giuseppe and Tompkins (2003b) examined a single deep convective scene using output from Tompkins (2001) and documented biases in reflectance of up to 16% when horizontal photon transport is neglected. On the other hand, Barker et al. (1998, 1999) contradicted this, using cloud scenes generated by cloud resolving and regional models. Barker et al. (2003) also showed the vast range of possible biases for different cloud regimes and emphasized the large disparities between various GCM radiation schemes if applied to complex cloud geometry, such as their open cell and deep convective simulations.

In discussing these contrasting claims, Di Giuseppe and Tompkins (2003b) noted that the models used by Barker et al. (1998, 1999) produced high cloud cover, representative of organized convective systems. Instead, the anvil cloud cover in the situation of isolated convective events modeled by Tompkins (2001) was only around 15%, with convective anvils reaching 20 to 30 km in diameter; perhaps more representative of isolated thunderstorms or unorganized convective situations.

The conflicting claims of Barker et al. (1998, 1999), Fu et al. (2000), and Di Giuseppe and Tompkins (2003b) highlight the weakness of this methodology where the bias is determined for individual and unrelated scenes. It would be preferable to study the evolution of radiative biases more systematically, where features of the cloud scene such as cirrus anvil cloud cover could be altered in isolation from other cloud properties. The reason that this has generally not been performed is the difficulty of controlling the cloud taxonomy and organization through model parameters and boundary conditions. Idealized models offer a much greater degree of control over the cloud scene, but so far they have only been successfully applied to the modeling of shallow, single-layer systems (Barker and Davies 1992; Cahalan et al. 1994; Petty 2002; Di Giuseppe and Tompkins 2003a), and are presently unable to provide realistic representations of complex scenes typifying deep convective situations.

Here a simple alternative methodology is adopted. A series of cloud scenes generated by a CRM are subject to modification by an idealized function, which allows the cirrus anvil coverage to be progressively enlarged without affecting the realism of the scene produced, offering controlled phase space investigation.

This paper first introduces the methodology, in addition to the radiative modeling assumptions and diagnostics. The bias resulting from the neglect of horizontal photon transport is then examined for the generated series of scenes in section 3. The bias observed consists of two contributions: the geometrical increase in fractional coverage due to cloud shading at low sun angles and the true 3D effect of photon scattering in the horizontal plane. Section 4 then attempts to account for the former geometrical contribution to the 1D bias by performing a simple correction technique, whereby the field is sheared by the tangent of the solar zenith angle (SZA), suggested by Varnai and Davies (1999). Section 5 discusses the implications of the findings, and considers possibilities for the future parameterization of these biases, while section 6 draws the conclusions.

2. Methodology

a. Radiation model

Here, only brief details of the radiative model and assumptions are given; for further information, the reader should refer to the description of Di Giuseppe and Tompkins (2003a). The investigation uses the Monte Carlo code outlined by Scheirer and Macke (2001). As in Di Giuseppe and Tompkins (2003a), a six-band calculation is performed for the spectral range of 0.2 to 4 microns, implemented with the *k*-distribution model of Fu and Liou (1992). The only three-dimensional field is the cloud mass mixing ratio; other quantities are a function of height only.

Mie theory is used for both water and ice, and particles concentrations of 50 and 30 cm^{-3} for water and ice, respectively, are adopted. Modeling the particle distribution using a Gamma function, this results in an effective radius range between 0.5 and 25 microns for the water droplets and 10 and 50 microns for the ice crystals. From the large range of possible habits, Field et al. (2003) found that the lack of sensitivity of the scattering phase function to measurement crystal diameter from aircraft observations in cirrus indicated that the spherical assumption for ice crystals can be a poor approximation [also, see habit examples in precipitating cirrus anvils in Heymsfield et al. (2002)]. However, Field et al. (2003) showed that the mean scattering properties and single scattering albedo of spherical particles compared reasonably well with the observations, better in fact, than a number of the other single-habit assumptions. It appears likely that a habit ensemble approach is more appropriate, advocated by Baran et al. (2001) and McFarquhar et al. (2002). The caveat of the simple spherical ice assumption is noted, and the sensitivity of one-dimensional radiative biases to the uncertainty of single scattering properties is left to future work.

For each cloud scene, two radiative calculations are performed: a full 3D solution and an independent col-

umn approximation (ICA) in which horizontal photon transport is inhibited, sometimes referred to as the independent pixel approximation (IPA). The ICA calculation is performed by imposing local periodic boundary conditions for each separate column of the CRM domain. Investigations are performed for a range of SZAs of 0° , 30° , 60° , and 75° .

b. CRM data

An ensemble of four CRM fields are used (from Tompkins 2001), which are separated by 6 h, with the ensemble members denoted as Exp-6, Exp-12, Exp-18, and Exp-24, respectively. The 3D fields have a horizontal dimension of approximately 90 km, with a horizontal resolution of 350 m. The second line of Fig. 1, labeled Exp-24:0, gives a representation of a typical CRM scene taken 24 h into the simulation (a minor adjustment has been made to the raw CRM field that is detailed below). The left column shows a planar view obtained by integrating the liquid and ice water in each column. In the right column a projection of the cloud field on the $Y = 0$ plane is shown. The other three ensemble members' cloud fields taken at 6, 12, and 18 h into the CRM simulation had contrasting arrangements of the clouds within the domain, but are quantitatively similar in terms of cloud structure and anvil cloud cover (not shown). Each of these four ensemble member fields is processed to give a range of cloud anvil coverages.

Over a given region that is assumed to be partially cloudy, with temperatures above the melting point, the horizontal distribution of temperature and total water (the sum of the water vapor and cloud liquid water) will be nonuniform. Considering the total water, in the clear sky the inhomogeneity is expressed in terms of water vapor fluctuations, while in cloudy regions the air is exactly saturated, and the variability is solely in cloud water. This is a consequence of the absence of significant supersaturation with respect to liquid water in the atmosphere, and the fast evaporation time scale. If the mean total water is uniformly increased in this layer, then part of the domain that was close to saturation will become cloudy as a result. Thus, by artificially increasing or decreasing the mean of the total water content, the cloud cover over this layer can be controlled, while the horizontal variability of the total water remains unchanged.

This approach is used to control the anvil cloud coverage of the CRM scenes. The ice, liquid, and vapor are combined to give the mean total water at each height. An idealized function, F , is added to the mean, and then the cloud water is diagnosed at each grid point assuming no supersaturation can exist. This latter assumption obviously involves a level of approximation for the ice phase, where supersaturation is commonplace (Heymsfield and Miloshevich 1995; Gierens et al. 2000). Converting supersaturation to ice (the adjustment involved in Fig. 1, Exp-24:0) increases anvil cov-

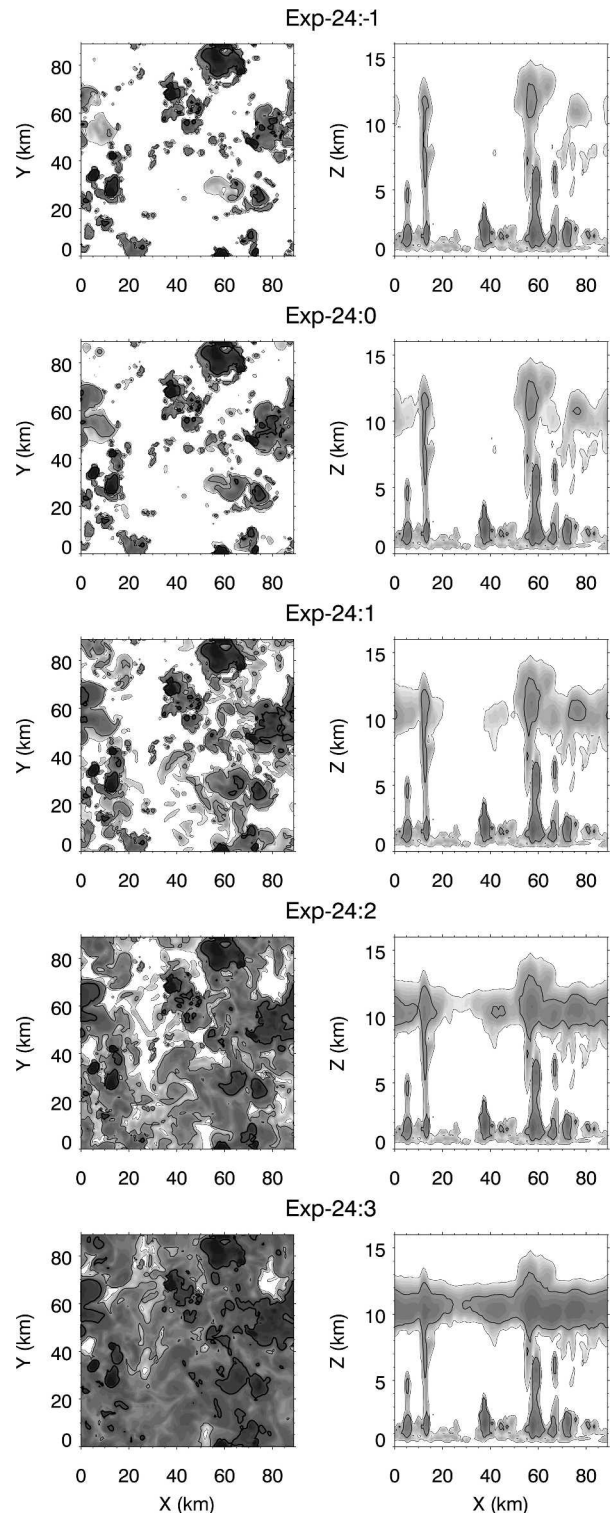


FIG. 1. Cloud fields generated from the Exp-24 CRM cloud scene. The five rows show processed fields using values of $K = -1, 0, 1, 2,$ and 3 (see text for details) and are labeled Exp-24: K : (left) planar view of total column integrated liquid plus ice water content (solid contours corresponding to $10, 100$ and 1000 gm^{-2}); (right) transect through cloud field at $Y = 0$ of the cloud water content [$\rho (q_i + q_l)$] (solid contours corresponding to 10^{-2} and 10^{-1} gm^{-3}).

erage from 15% to around 20%. However, while this will change radiative fluxes, the geometrical structure of the anvil cloud and the horizontal variability are not significantly altered, and thus this approximation is of minor importance for the assessment of radiative biases.

At each height, the cloud water mixing ratio q_c (the sum of cloud ice q_i and liquid water q_l mixing ratios) at each grid point in the horizontal is given by

$$q_c = \underbrace{K \mathcal{H}(z - z_1) \mathcal{H}(z_2 - z) 0.1 \overline{q_{\text{sat}}}}_F \sin^2 \left[\frac{(z - z_1)}{(z_2 - z_1)} \pi \right] + q_v + q_l + q_i - q_{\text{sat}}, \quad (1)$$

where the first term on the right is the idealized perturbation, denoted F , which is a function of height only, and is restricted to the layer residing between $z = z_1$ and $z = z_2$ by the application of the Heaviside function, \mathcal{H} . The constant K determines the maximum amplitude of the perturbation. The sine factor ensures the adjustment is introduced smoothly, while the scale factor $0.1 \overline{q_{\text{sat}}}$ (with q_{sat} specifying the saturation mixing ratio and the overbar representing the horizontal domain mean) allows K to adopt values of order unity.

Cloud water needs to be divided into liquid and ice, since this information is lost in the above process. For simplicity, this is accomplished diagnostically, with all cloud water treated as liquid above 0°C and ice below -23°C . Between these two threshold temperatures, the ice fraction varies linearly with temperature. The thresholds are similar to those given by Simmons et al. (1999) and reproduce the balance of the CRM data well.

For each of the four CRM input scenes, a series of five cloud fields is generated by specifying $K = -1$ (a cloud cover reduction); $K = 0$ (minor change due to the saturation adjustment); 1, 2, and 3, with $K = 3$ rendering the scene virtually overcast. The height of the adjustment is restricted to cirrus outflow region by imposing $z_1 = 8$ km and $z_2 = 12$ km. The five scenes generated from Exp-24 are given in Fig. 1, for $K = -1, 0, 1, 2,$ and 3 . With $K = -1$, the cirrus anvil dimensions are on the order of 10 km and do not spread far from the updraft cores. This scene could be representative of deep convection occurring in regions relatively dry in the upper troposphere, where detrained ice would sublimate on relatively short time scales. As K increases, the anvil dimension does so in tandem, with most of the domain already covered by at least thin cirrus with $K = 2$.

By design, the change in cloud cover is only due to cirrus anvil dimension. Note that while this method preserves the horizontal variance of total water for all ensemble members, this is unlikely to accurately reflect observed variances in contrasting scenes of low and high cirrus anvil cover, since microphysical processes such as ice sedimentation are likely to vary significantly between such situations. However, it is desirable for the

idealized tests conducted here to systematically change one parameter (cloud cover) in isolation from others such as total water variance. The variability of cloud ice water content will of course be affected, but Fig. 2 confirms that the shape of the probability density function (PDF) of the cloud ice in the middle of the cirrus anvil cloud at a height of 9.75 km is not radically altered.

The variability in cloud fraction between the four ensemble members is considerably smaller than the change in cloud fraction with K . The results are therefore presented as a function of the mean cloud fraction over the four ensemble members, effectively as a function of K . In Fig. 3, the vertical profiles for the idealized perturbation F and the adjusted cloud water content and cloud cover are shown for the Exp-24 case. In particular, the cloud cover is seen to range from around 10% to virtually overcast. The sensitivity to changing K is similar in the other three ensemble member scenes.

3. Mean solar biases

a. Effect of cloud cover

The mean ICA biases (defined as 3D-ICA/ICA as in Cahalan et al. 1994) are presented as a function of cloud cover and SZA in Fig. 4, and are stated in terms of a relative bias in percent. The ICA bias is identically zero for horizontally homogeneous clear sky conditions. For all other points the bias is presented as a function of the ensemble mean cloud fraction for a given value of K , with error bars representing one standard deviation of the bias over the four ensemble members.

The first notable feature of the bias curves is the strong dependence on cloud cover. From a zero bias for a clear-sky scene, the bias increases strongly with cloud cover to reach a maximum at a cloud cover of around 30% for reflectance. The maximum value of the bias is

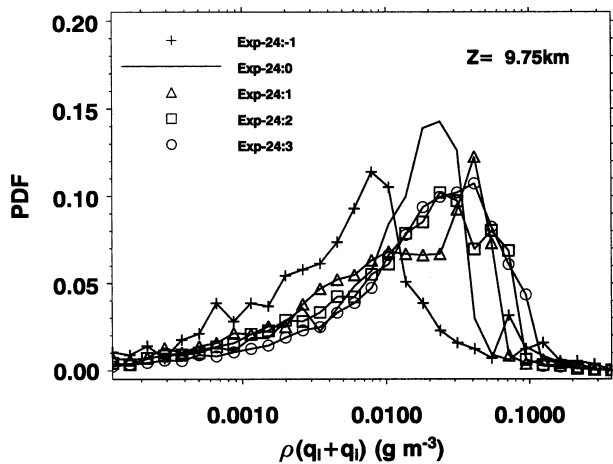


FIG. 2. PDF of the cloud water content field at a height of 9.75 km for scene Exp-24 modified by the full range of K values, labeled Exp-24: K .

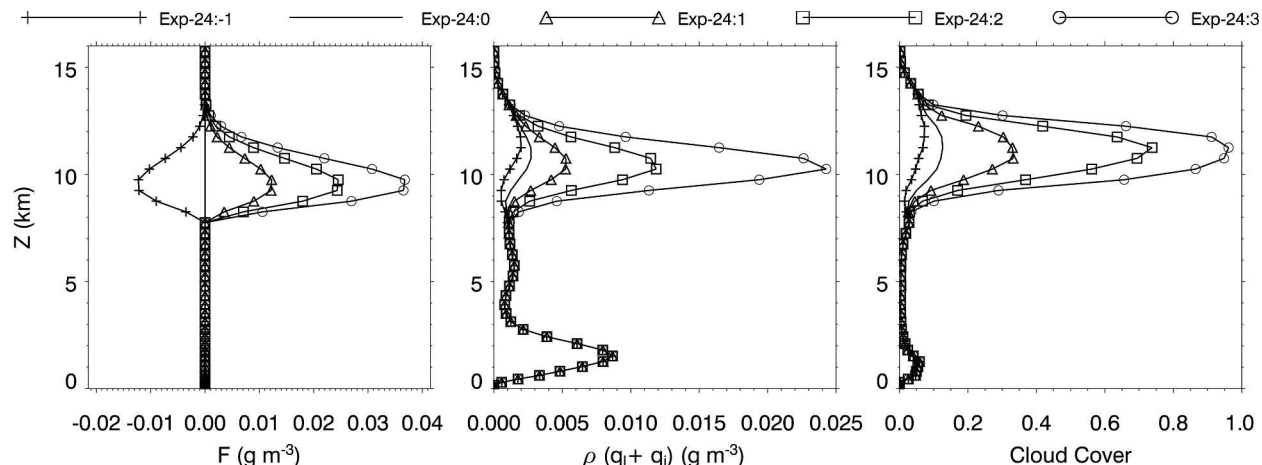


FIG. 3. Vertical profiles for the idealized cloud water perturbation F , the cloud water content $[\rho(q_i + q_l)]$, and the cloud cover for the Exp-24 case.

around 20% when the sun is overhead, but is larger when the sun is low, reaching as much as 46% for a SZA of 75° . After the peak bias is reached, it begins to fall off more slowly with cloud cover, approaching zero as the scene becomes overcast. The transmittance and absorptance profiles are similar to those of the reflectance. It should be noted that these conclusions are based on relative biases, giving an estimate of the accuracy of the ICA calculation. However, in terms of absolute energy, the conclusions are unaltered, with the largest bias found at the SZA of 75° , despite the scaled incoming solar radiation.

Using this systematic documentation of the bias as a function of cloud cover, it is possible to place the previous investigations using cloud resolving model input into context. Di Giuseppe and Tompkins (2003b) documented biases of 16% for a scene with cloud cover peaking at around 15% in the anvil region. On the other hand, the investigations of Barker et al. (1998, 1999) documented significantly smaller biases of less than 5% for scenes approaching overcast conditions, even for low sun angles. Here it is revealed that for a SZA of 60° , the bias is also less than 5% when the cloud cover exceeds 80%. Barker et al. (2003) documented the maximum biases of around 10% in the most geometrically complex case of deep convection with a cloud cover of 45%.

Figure 4 highlights, therefore, the dangers of studying isolated scenes and generalizing these results to wider dynamical scenarios. The convective scenes with cloud cover exceeding 90% studied by Barker et al. (1999) may be representative of organized convective scenes with cloud shields extending many hundreds if not thousands of kilometers, and the results here appear to confirm the ICA biases are likely to be limited in such scenarios. However, generalizing these results to conclude that ICA biases are unimportant in all convective situations is likely to underestimate the importance of

3D effects. Likewise, Di Giuseppe and Tompkins (2003b) and Fu et al. (2000) with their relatively sparse cloud scenes of low cloud cover, also underestimated the maximum possible ICA bias.

b. Effect of cloud number

The obvious question that arises from Fig. 4 is why the bias peaks at a cloud cover of 30% rather than at higher or lower values. Since the bias is such a strong function of cloud cover, it is likely that cloud geometry is playing a role, and more specifically, the number, organization, and interaction between clouds inside the domain.

Varnai and Davies (1999) systematically itemized the variety of photon interaction mechanisms that can play a role in 3D radiative transfer. Their taxonomy included a number of (multiple) scattering-based effects such as photon trapping and escape mechanisms that are not treatable in a 1D calculation. Collectively, these scattering effects were complemented by the additional category of shading. The latter accounts for the fact that, even in the absence of scattering events, when the sun is low a photon will encounter a different cloud history from that assumed by a 1D method using a rescaled calculation with the sun overhead (see their Fig. 4). In a three-dimensional geometry the shading effect will produce filling of clear-sky regions between separate clouds with consequent enhancement of the effective cloud cover. This mechanism becomes more efficient with increasing cloud number (with associated increasing gaps and cloud boundaries) and lower sun angles. It is thus apparent from their analysis that two clouds at the same altitude of a certain horizontal dimension separated by a clear-sky gap are likely to have a larger 3D effect than one single cloud of a size equivalent to their sum.

To picture how the bias portrayed in Fig. 4 is related to the geometrical cloud organization, a simple thought

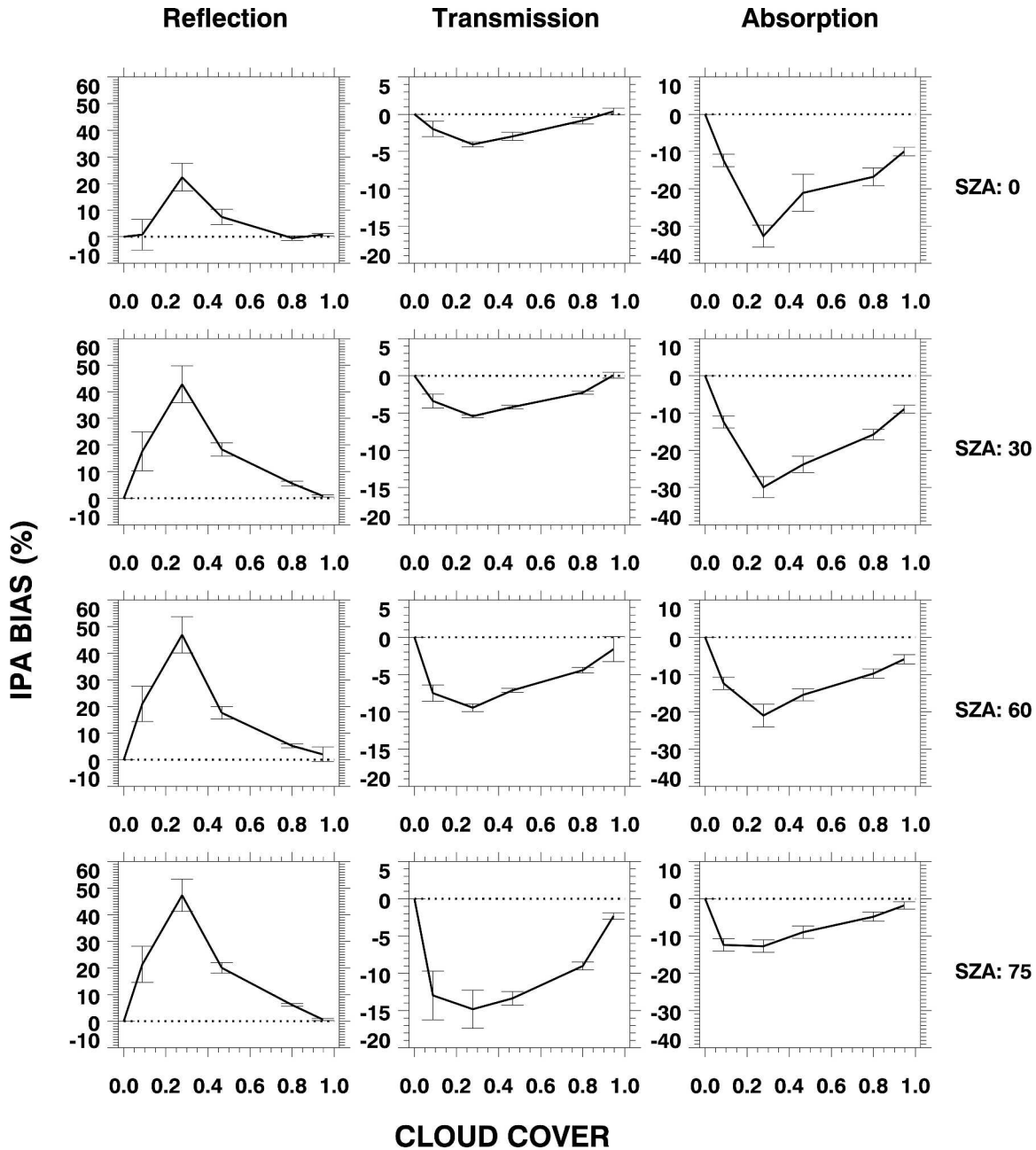


FIG. 4. Relative ICA biases (y axis in %) as a function of cloud cover and SZA ($^{\circ}$). The error bars represent one standard deviation of the bias over the four ensemble members.

experiment is suggested starting from clear-sky conditions and then progressively increasing cloud cover by adding individual clouds of a specific size one at a time. At first, since the cloud cover is low, each new cloud is unlikely to overlap with an existing one and the number of clouds and cloud cover will both grow. The magnitude of 3D radiative effects will increase in tandem, and thus also the 1D bias arising from their neglect. As the cloud cover increases, the probability that a new cloud will overlap with an existing one is larger. The cloud

cover will reach a point at which the addition of new clouds will not increase the population since they will overlap existing clouds, or even reduce the number by joining existing clouds; the limit being an overcast sky (essentially one cloud). Thus there will exist a scene cloud cover at which the number of separate, isolated cloud elements is at a maximum, for which the 1D bias will presumably be greatest.

The number of separate clouds and their mean cloud horizontal dimension at the cirrus anvil level for the

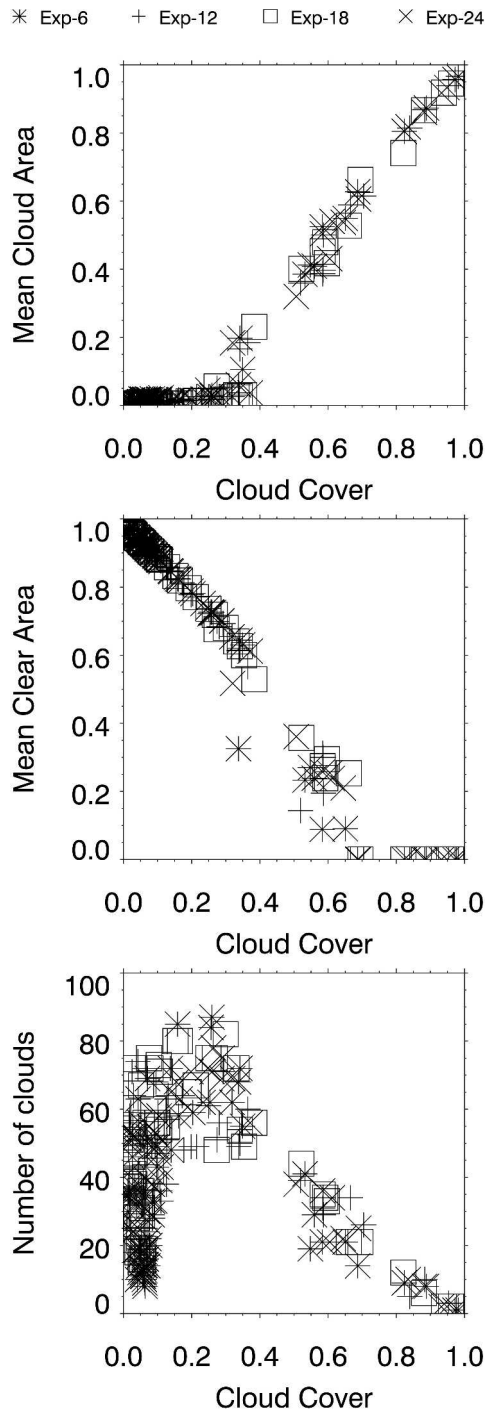


FIG. 5. Statistics of the cloud cover as a function of (top to bottom) the cloud area dimension, the clear gap dimension, and the total cloud numbers for Exp: $K=6, 12, 18,$ and 24 . The analysis is performed for the all four CRM scenes at heights between $z_1 = 8$ km and $z_2 = 12$ km.

four ensemble members are diagnosed (Fig. 5). This is accomplished by identifying a cloudy pixel if the cloud water mixing ratio exceeds a 10^{-4} kg^{-1} threshold. All connecting cloud points are recursively identified and

allocated to the same cloud. This analysis is performed for all model layers throughout the cirrus anvil region and for all twenty cloud scenes analyzed. Figure 5 shows that at first the mean cloud dimension (normalized to the scene area) stays constant as the cloud cover increases, but at the point where the maximum in 1D radiative biases was noted the cloud dimension sharply increases, as clouds start to join to form larger dimension shields. In agreement with this statistic, the lowest panel illustrates that this cloud cover of around 30% coincides with the maximum of the number of cloud elements.

This observation indicates a diagnostic, the number of separate clouds or equivalently the cloud boundary to volume ratio, which a parameterization of 1D biases may be based on, at least in such a quasi-2D framework that the cirrus anvil deck represents where the horizontal scale of the cloud greatly exceeds its vertical extent. The increase in total cloud cover when randomly adding a cloud of fractional area A to a scene with cover C is simply given by $A(1 - C)$, which is used in the treatment of convective detrainment in GCMs that utilize a prognostic cloud cover equation (e.g., Tiedtke 1993). Predicting the number of cloud elements is more complex, since it depends on the PDF of the subgrid-scale fluctuations of temperature and humidity, and additionally how those fluctuations are arranged within the domain.

To investigate the sensitivity of the cloud number PDF, the spectral, idealized, thermodynamically consistent model (SITCOM) of Di Giuseppe and Tompkins (2003a) is used to generate a series of single-layer cloud scenes with cloud cover ranging from zero to 100% by altering the saturation mixing ratio (see Di Giuseppe and Tompkins, 2003a, for further details of SITCOM). The number of separate clouds as a function of cloud cover is then ascertained. The fluctuations of the total water are described by a power-law spectra with a long wavelength cutoff (Di Giuseppe 2005). The sensitivity to the PDF is investigated by using a power-law slope ranging from -1 (white noise) through $-5/3$ to -3 , covering the observed range (Benner and Curry 1998). The cloud number as a function of cloud cover is shown in Fig. 6 for the three power-law slopes, along with the CRM results. It is seen that the cloud cover at which the maximum cloud number occurs is insensitive to the power-law slope and even for the extreme case of white noise fluctuations, the peak only moves from around 26%–32%. Thus it would appear that if the variance of the total water fluctuation is known, which may be provided in a GCM by a statistical parameterization (e.g., Bougeault 1982; Bony and Emanuel 2001; Golaz et al. 2002; Tompkins 2002), then a parameterization for the ICA bias may reasonably assume a fixed-slope power-law spectra for the fluctuations.

4. Bias correction

The cloud number-related ICA bias documented in the previous section must be the result of a combination

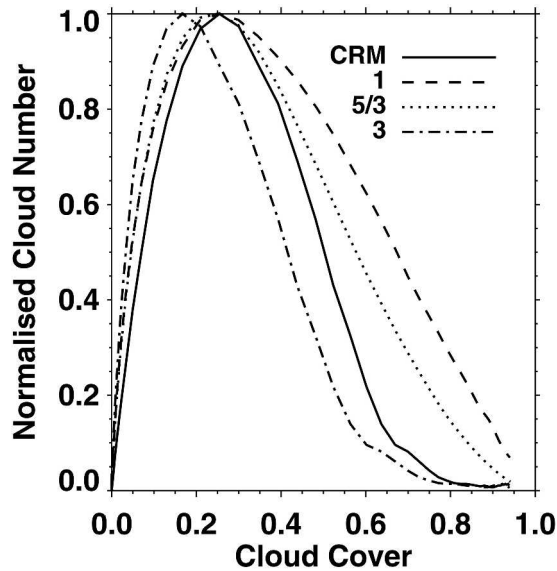


FIG. 6. Cloud number as a function of cloud cover, calculated with a statistical model using three power law slopes, marked K in the caption, where $-K$ is the power law slope used. CRM fields are shown for comparison.

of scattering and shading effects discussed by Varnai and Davies (1999). In contrast to the complication of parameterizing the consequences of 3D scattering processes in a 1D framework, the shading effect is merely a geometrical factor and can be tackled relatively straightforwardly. Varnai and Davies (1999) outlined a

variant of the ICA calculation, termed the tilted ICA (TICA), where each column of an ICA calculation is given the profile of cloud condensate and clear-sky gaps encountered by a direct ray from the sun. Practically, this can be approximated by applying a lateral translation of the cloud field by a distance equivalent to the tangent of the solar zenith angle. In terms of this effect, a declining sun angle is no different radiatively than a physical translation of a cloud deck by vertical wind shear (as stated by Barker 1994).

The TICA approximation is applied here to assess by how much, if any, it reduces the bias of the orthodox ICA methodology. The calculation is accomplished for all sun angles and cloud covers for ensemble member Exp-24. Figure 7 shows how the TICA calculation shears the Exp-24:0 cloud scene and increases the effective cloud cover for low sun angles. The total cloud cover in the sun overhead case is increased to 0.45 when the SZA is 75° . It is apparent how the translated field enables the ICA calculation to appreciate not only the increased shading of clouds by their neighbors at low sun angles, but also to take the enhanced illumination of exposed cloud sides into account.

Comparing the TICA and ICA biases (Fig. 8), when the sun is overhead the TICA obviously applies no correction and the calculations are identical. However, as the sun angle progressively increases, the bias for both the reflectance and transmittance increases for the ICA, since not only is the scattering neglected, but the geometry of the sun angle also plays an increasing role. As the sun declines from the overhead position to its

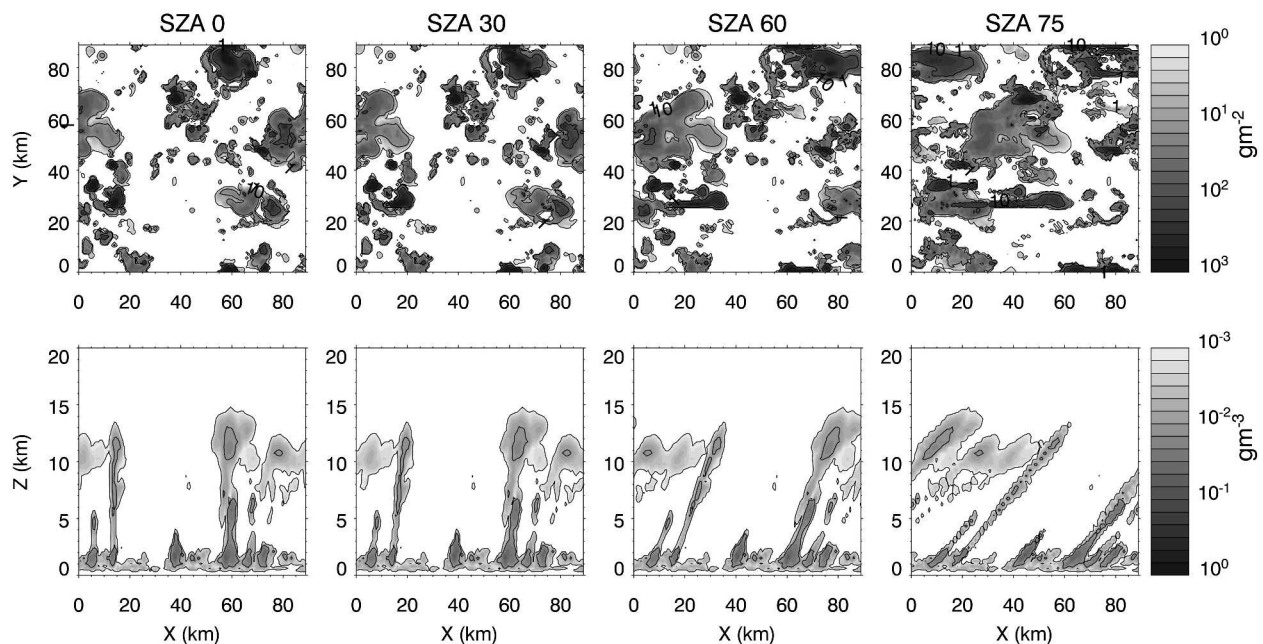


FIG. 7. As per Fig. 1, (top) column integrated and (bottom) x - z average cloud water for the Exp-24:0 scene modified by the TICA approach.

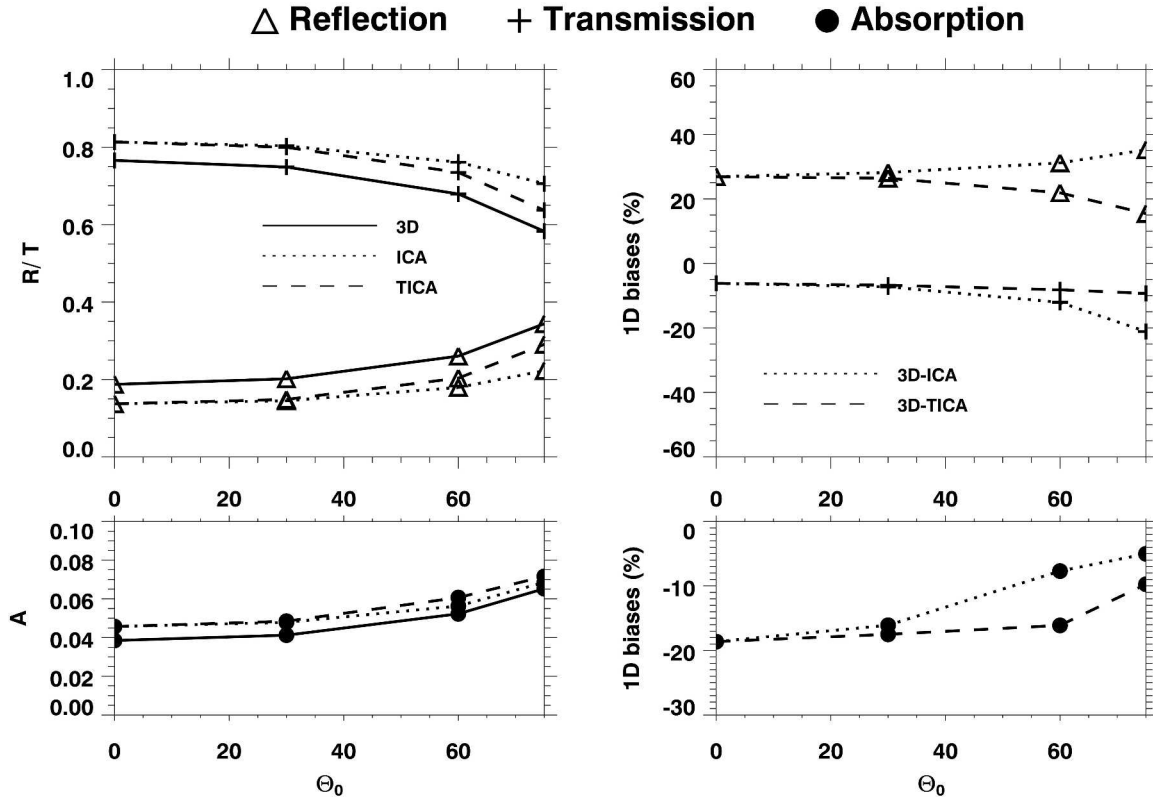


FIG. 8. (left top) Reflection, transmission, and (left bottom) absorption vs solar angle for 3D, ICA, and TICA calculations for the Exp-24:0 cloud scene. Relative biases for the ICA and TICA calculation (right top) reflection, transmission, and (right bottom) absorption vs solar angle.

lowest angle of 75° , the 3D reflectance increases from 0.19 to 0.35. The increase for the ICA is far more modest: rising from 0.14 to 0.21. In sharp contrast, the TICA manages to mimic the increase in reflectance of the 3D calculation well, with reflectance changing from 0.14 to 0.29 as the sun descends. The TICA bias actually reduces for lower sun angles and at a SZA of 75° , it is able to correct for more than half of the ICA bias in reflectance. The same conclusions hold for the transmittance.

Examining the percentage correction to the ICA bias made by the TICA approach, the latter is able to correct the bias in reflectance over a wide range of cloud covers (Fig. 9). If the TICA bias is entirely due to photon scattering, and the ICA bias is the consequence of both scattering and sun-angle geometry, then the ratio of the TICA to the ICA bias gives an estimate of the relevance of photon scattering to 1D biases. It is clear that all the bias is due to scattering when the sun is overhead. However, as the sun lowers, the contribution to the 1D biases due to the increase in cloud cover is evident. In this regime, the TICA approach is able to correct for most of the bias, and can account for the increase in the cloudy area due to the three-dimensional geometry even if it is a one-dimensional solution, assuming of course that one has knowledge of the cloud locations.

The contribution due to the true scattering is fairly limited and mostly independent of the cloud cover and the sun zenith angle for this case. At a SZA of 75° , the scattering effect accounts for around 5% of the bias at a cloud cover of 30% (Fig. 9).

5. Discussion

The previous section showed that the scattering bias was approximately independent of SZA and that the geometrical effect can be tackled with the TICA approach. Can this conclusion be generalized to apply to all cloud regimes? The answer depends on the nature of the cloud field. If the mean photon pathlength is much smaller than the cloud horizontal dimension, the horizontal flux components are significantly reduced leaving only the vertical component. A quasi-2D geometry would therefore imply a modest contribution to the 1D bias resulting from horizontal fluxes.

Many cloud types are in fact quasi-2D in nature, as their meteorological nomenclature suggests. However, deep convective scenes are widely regarded as complex 3D phenomena, because of the presence of the updraft towers. The insensitivity of the scattering bias to SZA here indicates that the upright towers play a minor role

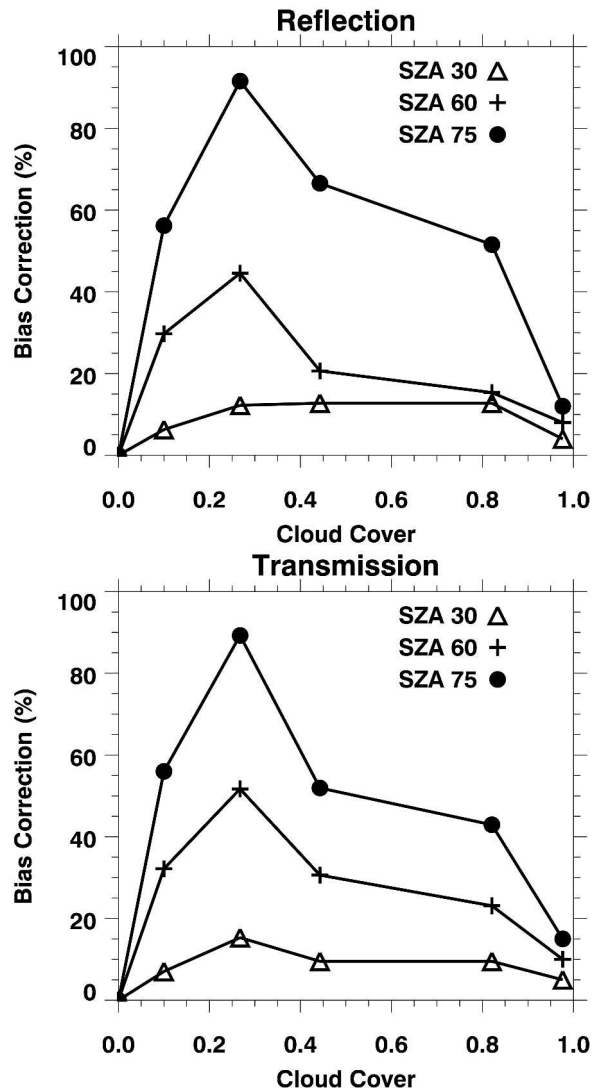


FIG. 9. Percentage of 1D bias correction for (top) reflection and (bottom) transmission due to the TICA approach as a function of the cloud cover and different SZAs.

radiatively speaking, and it is the effect of the quasi-2D convection-generated cirrus shield that dominates. As a forest would have limited radiative effect without its canopy, so would convective cloud scenes without their cirrus anvil outflow. Effectively, the 3D convective scenes can be considered a 2D single-layer cloud scene consisting of only the cirrus deck.

If most individual cloud regimes can thus be represented as quasi-2D single layers, this may simplify the task of parameterizing the radiative biases resulting from the neglect of photon scattering. However, further complications occur when different cloud regimes are combined to give a multilayer cloud scene, which has been rarely studied to date. In observations, roughly 30%–40% of cloud scenes are multilayer (Warren et al. 1985), but encouragingly, multilayer states usually con-

sist of only two layers with one of these layers usually occurring in the planetary boundary layer (PBL; Wang et al. 2000). If a PBL cloud is in the form of stratocumulus or stratus of high fractional cloud cover and limited vertical extent, ICA biases are limited (Cahalan et al. 1994; Di Giuseppe and Tompkins 2003b), perhaps simplifying the task of describing multilayer cloud scenes.

This is not to say these are the only factors that are important in the parameterization context when considering a GCM calculation. The GCM must, for example, make a decision concerning the arrangement of the cloud cover in the domain and how these elements overlap in the vertical. Instead, an ICA representation of the field has knowledge of both of these effects. This and other work demonstrates that it is not primarily the cloud cover, per se, that determines the magnitude of the 1D bias, but how this is arranged within the domain. The peak in bias occurred at roughly the cloud fraction where the number of cloud elements was maximized. If this cloud fraction were instead expressed as one continuous deck, as would be the case, for example, at the boundary of a frontal cloud in midlatitudes, then the 1D bias would likely be much smaller. The GCM must decide therefore, not only how the clouds overlap in the vertical, but also if the cloud fraction consists of one cloud or many smaller clouds; in other words, to consider the cloud organization. Di Giuseppe and Tompkins (2003a) showed how the spatial scale of cloud organization could play a role in 1D radiative biases in shallow cloud systems. Here it is illustrated how this is also the case in deep convective systems and that the potential error in its neglect can be far greater.

6. Conclusions

There has been considerable argument in the literature concerning the magnitude of the bias in solar radiative transfer calculations when horizontal photon transport is neglected, partly due to the various isolated cloud scenes with contrasting attributes used to assess this bias. The difficulty of obtaining a realistic set of cloud scenes for situations of complex cloud geometry, while certain characteristics such as total cloud cover are altered in isolation, has hindered attempts to reach a consensus.

Here an alternative and simple approach was adopted to systematically examine the relation of solar biases in deep convective regimes to the anvil cloud coverage. An ensemble of four cloud scenes generated by a cloud resolving model were subjected to modification by an idealized function that allows the cirrus anvil coverage to be progressively enhanced without affecting the realism of the scene produced.

It is found that the bias in scene albedo can reach as much as 22% when the sun is overhead and 46% at low sun angles. This maximum bias is attained at cirrus anvil

cloud cover of approximately 30% to 40%. The bias is an asymmetrical function of cloud cover. For cloud cover of around 15%, the bias is half its maximum value, while it is limited for coverage exceeding approximately 80%.

These findings corroborate earlier work for deep convective situations, where small biases were found in deep convective scenes with high cloud cover, while scenes with 20% coverage produced much more significant biases. The systematic nature of this investigation shows that these earlier studies were in fact not contradictory, and differed only because of the contrasting nature of the cloud scenes used.

The position of the peak in the bias, which was around 30% cloud cover for the CRM scene used here, coincides with the maximum number of independent clouds present in the scene. Increasing the cloud cover past this point reduces the bias, since the merging of clouds rapidly increases the mean cloud element size, effectively reducing the area of exposed cloud surfaces to the photon interaction. Sensitivity tests with an idealized model show that the cloud cover at which this peak occurs is relatively insensitive to changes in the slope of the power law describing the organizational scale of the clouds. Increasing the solar zenith angle exacerbates this effect by increasing the effective cloud cover.

While this effect is purely geometrical and does not account for the complex 3D nature of the scattering processes, it was shown that it provides the largest contribution to the total bias, at low sun angles. An attempt to correct for it is made by performing a simple technique, whereby the field is sheared by the tangent of the solar zenith angle. This technique was previously suggested and implemented by Varnai and Davies (1999). Here the technique is able to greatly reduce the 1D bias at low sun angles. The residual scattering bias is almost independent of SZA for this scene, and indicates that even apparently complex 3D deep convective cloud scenes can be considered in terms of only their quasi-two-dimensional cirrus anvil deck. This is encouraging, since it implies that most cloud regimes can be considered as quasi-2D layers, facilitating the effort to parameterize the scattering bias. To this end, models will have to take account of the organization of humidity and cloud fluctuations within the domain, in addition to the PDF describing their magnitude. This will be further complicated by interaction between layers in multilayer cloud regimes, which observations indicate encompasses 40% of all cloudy scenes.

Acknowledgments. This manuscript has benefited from comments provided by Jean-Jacques Morcrette. Ronald Scheirer and Andreas Macke are thanked for providing their Monte Carlo code GRIMALDI and advice on its use. The Met Office (United Kingdom) made available the cloud resolving model used to generate the cloud fields. Part of this research work was per-

formed while the first author was supported by NERC Studentship GT/4/00/217 at ESSC, University of Reading, United Kingdom

REFERENCES

- Aida, M. A., 1977: Scattering of solar radiation as a function of cloud dimension and orientation. *Quat. Spectrosc. Radiat. Transfer.*, **17**, 303–310.
- Baran, A. J., P. N. Francis, L. C. Labonnote, and M. Douciaux-Boucher, 2001: A scattering phase function for ice cloud: Test of applicability using aircraft and satellite multi-angle multi-wavelength radiance measurements of cirrus. *Quart. J. Roy. Meteor. Soc.*, **127**, 2395–2416.
- Barker, H. W., 1994: Solar radiative transfer for wind-sheared cumulus cloud fields. *J. Atmos. Sci.*, **51**, 1141–1156.
- , and J. A. Davies, 1992: Solar radiative fluxes for broken cloud fields above reflecting surfaces. *J. Atmos. Sci.*, **49**, 749–761.
- , and Z. Q. Li, 1997: Interpreting shortwave albedo-transmittance plots: True or apparent anomalous absorption? *Geophys. Res. Lett.*, **24**, 2023–2026.
- , J. J. Morcrette, and G. D. Alexander, 1998: Broadband solar fluxes and heating rates for atmospheres with 3D broken clouds. *Quart. J. Roy. Meteor. Soc.*, **124**, 1245–1271.
- , G. L. Stephens, and Q. Fu, 1999: The sensitivity of domain-averaged solar fluxes to assumptions about cloud geometry. *Quart. J. Roy. Meteor. Soc.*, **125**, 2127–2152.
- , and Coauthors, 2003: Assessing 1D atmospheric solar radiative transfer models: Interpretation and handling of unresolved clouds. *J. Climate*, **16**, 2676–2699.
- Benner, T. C., and J. A. Curry, 1998: Characteristics of small tropical cumulus clouds and their impact on the environment. *J. Geophys. Res.*, **103**, 28 753–28 767.
- Bony, S., and K. A. Emanuel, 2001: A parameterization of the cloudiness associated with cumulus convection; Evaluation using TOGA COARE data. *J. Atmos. Sci.*, **58**, 3158–3183.
- Bougeault, P., 1982: Cloud ensemble relations based on the Gamma probability distribution for the high-order models of the planetary boundary layer. *J. Atmos. Sci.*, **39**, 2691–2700.
- Cahalan, R. F., W. Ridgway, and W. J. Wiscombe, 1994: Independent pixel and Monte Carlo estimates of stratocumulus albedo. *J. Atmos. Sci.*, **51**, 3776–3790.
- Chambers, L. H., B. A. Wielicki, and K. F. Evans, 1997: Accuracy of the independent pixel approximation for satellite estimates of oceanic boundary layer cloud optical depth. *J. Geophys. Res.*, **102**, 1779–1794.
- Di Giuseppe, F., 2005: Sensitivity of one-dimensional radiative biases to vertical cloud structure assumptions: Validation with aircraft data. *Quart. J. Roy. Meteor. Soc.*, in press.
- , and A. M. Tompkins, 2003a: Effect of spatial organization on solar radiative transfer in three-dimensional idealized stratocumulus cloud fields. *J. Atmos. Sci.*, **60**, 1774–1794.
- , and —, 2003b: Three-dimensional radiative transfer in tropical deep convective clouds. *J. Geophys. Res.*, **108**, 4741, doi:10.1029/2003JD003392.
- Field, P. R., A. J. Baran, P. H. Kaye, E. Hirst, and R. Greenaway, 2003: A test of cirrus ice crystal scattering phase functions. *Geophys. Res. Lett.*, **30**, 1752, doi:10.1029/2003GL017482.
- Fu, Q., and K. N. Liou, 1992: On the correlated k -distribution method for radiative-transfer in nonhomogeneous atmospheres. *J. Atmos. Sci.*, **49**, 2139–2156.
- , M. C. Cribb, H. W. Barker, S. K. Krueger, and A. Grossman, 2000: Cloud geometry effects on atmospheric solar absorption. *J. Atmos. Sci.*, **57**, 1156–1168.
- Gierens, K., U. Schumann, M. Helten, H. Smit, and P. H. Wang, 2000: Ice-supersaturated regions and subvisible cirrus in the northern midlatitude upper troposphere. *J. Geophys. Res.*, **105**, 22 743–22 753.
- Golaz, J., V. E. Larson, and W. R. Cotton, 2002: A PDF-based

- parameterization for boundary layer clouds. Part I: Method and model description. *J. Atmos. Sci.*, **59**, 3540–3551.
- Heymsfield, A. J., and L. M. Miloshevich, 1995: Relative humidity and temperature influences on cirrus formation and evolution: Observations from wave clouds and FIRE II. *J. Atmos. Sci.*, **52**, 4302–4326.
- , A. Bansemer, P. R. Field, S. L. Durden, J. L. Stith, J. E. Dye, W. Hall, and C. A. Grainger, 2002: Observations and parameterizations of particle size distributions in deep tropical cirrus and stratiform precipitating clouds: Results from in situ observations in TRMM field campaigns. *J. Atmos. Sci.*, **59**, 3457–3491.
- Marshak, A., A. Davis, W. Wiscombe, and R. F. Cahalan, 1997: Scale invariance in liquid water distributions in marine stratocumulus. Part II: Multifractal properties and intermittency issues. *J. Atmos. Sci.*, **54**, 1423–1444.
- McFarquhar, G. M., P. Yang, A. Macke, and A. J. Baran, 2002: A new parameterization of single scattering solar radiative properties for tropical anvils using observed ice crystal size and shape distributions. *J. Atmos. Sci.*, **59**, 2458–2478.
- McKee, T. B., and S. K. Cox, 1974: Scattering of visible radiation by finite clouds. *J. Atmos. Sci.*, **31**, 1885–1892.
- O'Hirok, W., and C. Gautier, 1998: A three-dimensional radiative transfer model to investigate the solar radiation within a cloudy atmosphere. Part I: Spatial effects. *J. Atmos. Sci.*, **55**, 2162–2179.
- Petty, G. W., 2002: Area-averaged solar radiative transfer in three-dimensionally inhomogeneous clouds: The independent scattering cloudlet model. *J. Atmos. Sci.*, **59**, 2910–2929.
- Scheirer, R., and A. Macke, 2001: On the accuracy of the independent column approximation in calculating the downward fluxes in the UVA, UVB and PAR spectral ranges. *J. Geophys. Res.*, **106**, 14 301–14 312.
- Simmons, A. J., A. Untch, C. Jakob, P. Kallberg, and P. Undén, 1999: Stratospheric water vapour and tropical tropopause temperatures in ECMWF analyses and multi-year simulations. *Quart. J. Roy. Meteor. Soc.*, **125**, 353–386.
- Tiedtke, M., 1993: Representation of clouds in large-scale models. *Mon. Wea. Rev.*, **121**, 3040–3061.
- Tompkins, A. M., 2001: Organization of tropical convection in low vertical wind shears: The role of cold pools. *J. Atmos. Sci.*, **58**, 1650–1672.
- , 2002: A prognostic parameterization for the subgrid-scale variability of water vapor and clouds in large-scale models and its use to diagnose cloud cover. *J. Atmos. Sci.*, **59**, 1917–1942.
- Varnai, T., and R. Davies, 1999: Effects of cloud heterogeneities on shortwave radiation: Comparison of cloud top variability and internal heterogeneity. *J. Atmos. Sci.*, **56**, 4206–4224.
- Vogelmann, A. M., V. Ramanathan, and I. A. Podgorny, 2001: Scale dependence of solar heating rates in convective cloud systems with implications to general circulation models. *J. Climate*, **14**, 1738–1752.
- Wang, J., W. B. Rossow, and Y. Zhang, 2000: Cloud vertical structure and its variations from a 20-yr global rawinsonde dataset. *J. Climate*, **13**, 3041–3056.
- Warren, S. G., C. J. Hahn, and J. London, 1985: Simultaneous occurrence of different clouds types. *J. Appl. Meteor.*, **24**, 658–667.
- Zuidema, P., and K. F. Evans, 1998: On the validity of the independent pixel approximation for boundary layer clouds observed during ASTEX. *J. Geophys. Res.*, **103**, 6059–6074.